j mater res technol. 2016;xxx(xx):xxx–xxx

Available online at www.sciencedirect.com

jmr&t Journal of Materials Research and Technology

www.jmrt.com.br

Original Article

Study of the corrosion behaviour of S32101 duplex and 410 martensitic stainless steel for application in oil refinery distillation systems

Roland T. Loto[a,b]

[a] *Department of Mechanical Engineering, Covenant University, Ota, Ogun State, Nigeria*

[b] *Department of Chemical, Metallurgical & Materials Engineering, Tshwane University of Technology, Pretoria, South Africa*

ARTICLE INFO

Article history:
Received 3 August 2016
Accepted 10 November 2016
Available online xxx

Keywords:
Corrosion
Duplex
Martensitic
Hydrochloric
Steel

ABSTRACT

The corrosion behaviour of S32101 duplex and 410 martensitic stainless steel was studied through weight loss and potentiodynamic polarization in 1–6 M HCl solutions. Results show that S32101 steel has significantly lower corrosion rates than 410 steel from both tests at all concentrations with highest values of 0.04586 mm/y and 0.234 mm/y in comparison to martensitic steel with corrosion rates of 0.827 mm/y and 19.84 mm/y at 6 M HCl concentration. Micrographs from SEM and EDS analyses showed a less corroded morphology for S32101 steel with fewer pits and slight depletion in the percentage composition of chromium and other alloying elements.

© 2016 Brazilian Metallurgical, Materials and Mining Association. Published by Elsevier Editora Ltda. This is an open access article under the CC BY-NC-ND license (http://creativecommons.org/licenses/by-nc-nd/4.0/).

1. Introduction

Stainless steels are corrosion-resistant ferrous metals due to the thin, protective film formed on its surface, a combination of iron and chromium compounds. The film being passive protects the steel from corrosion coupled with the property of self-healing. The presence of chromium within the steel microstructure significantly enhances their corrosion resistance. Research by Hashimoto et al. [1] showed that the protective film consists of chromium oxy-hydroxide. Its durability with respect to corrosion resistance depends on the percentage content of chromium and other alloying elements responsible for its stainless metallurgical structure. As a result chromium–nickel stainless steels are currently the most extensively applied materials in corrosive environments both at ambient and elevated temperatures, however they are prone to localized corrosion such as pitting in the presence of chloride or other aggressive anions [2–5]. Pitting corrosion is one of the most major causes of deterioration of stainless steel in petrochemical industries [6].

The petrochemical industry coupled with its difficult production operations experiences huge corrosion problems. Corrosion, the degradation of a metal or alloy and its inherent properties, destroys most parts/component at every stage within the industry [7,8]. The major causes of corrosion in the oil industry are chlorides, carbon dioxide, ammonia, hydrogen chloride, sulfuric acid, hydrogen, sulphur, etc. Within the industry corrosion in crude distillation overhead systems is a recurrent problem in refineries due to the presence of acid

E-mail: tolu.loto@gmail.com

http://dx.doi.org/10.1016/j.jmrt.2016.11.001

2238-7854/© 2016 Brazilian Metallurgical, Materials and Mining Association. Published by Elsevier Editora Ltda. This is an open access article under the CC BY-NC-ND license (http://creativecommons.org/licenses/by-nc-nd/4.0/).

Please cite this article in press as: Loto RT. Study of the corrosion behaviour of S32101 duplex and 410 martensitic stainless steel for application in oil refinery distillation systems. J Mater Res Technol. 2016. http://dx.doi.org/10.1016/j.jmrt.2016.11.001

which attacks component structures. Under-deposit corrosion and fouling from acid neutralization and desalter operations is also responsible for component deterioration and breakdown. In the crude overhead systems the corrosion is due to the presence of HCl acid vapor present from hydrolysis of salts in the atmospheric crude distillation unit. The major source of HCl is the hydrolysis of calcium and magnesium chloride salts at temperatures 121 °C and the decomposition of organic chloride compounds [9–18]. HCl is generally the most complex acid to control from the corrosive point of view. It requires extraordinary precaution during its use and in the selection of materials to contain the acid. It is highly corrosive to most of the common metals and alloys [19]. HCl moves into the crude unit overhead condensing systems where it is readily absorbed into condensing water.

Some HCl boils overhead in the fractionating column and dissolves in the water as it precipitates in the condenser. The resulting low pH water, being very corrosive causes frequent overhead condenser tube failures. Hydrogen chloride also condenses in the heat exchanger in the atmospheric fractionating column overhead forming highly corrosive hydrochloric acid [20,21]. Other acids such as sulfur-oxide compounds and organic acids contribute to corrosion in addition to conditions that upsets the process conditions resulting higher acid content which causes the dissolution of protective iron sulfide/hydroxide scales [17].

At present the cost of corrosion is estimated on the order of 3–4% of gross domestic product (GDP) of developed countries necessitating so many studies on it and the development of corrosion resistant alloy materials to reduce its impact and consequences [21,22]. Duplex stainless steels are the steels developed with high strength and chloride stress corrosion cracking resistance in aggressive environments. It has high chromium content with other alloying elements which provides good resistance to localized and general corrosion coupled good fatigue strength, pitting formation resistance, good machinability and weldability. The steel consists of balanced ferrite and austenite phases coupled with versatile applications where good corrosion resistance and mechanical properties are required. They are used in biodiesel and ethanol plants and tanks, waste water handling systems, ethanol production components, desalination system chambers and evaporators, chemical processing, pressure vessels, piping, heat exchangers, etc. It is highly suitable for service in environments containing chlorides and hydrogen sulfide, such as marine applications and the oil and gas extraction and processing industries and mining industries [23,24]. Martensitic stainless steels are general-purpose steels containing chromium, which provide good corrosion resistance properties. They are generally used for applications involving mild corrosion, heat resistance; adequate ductility, toughness and high strength such as in are used in various industries such as in chemical plants, power generation equipments in gas turbines and compressor blades and discs, aircraft engine components and fittings in marine components [25]. Numerous researches have been done to evaluate the corrosion resistance and susceptibility of duplex and martensitic stainless steel in corrosive environments. Souto et al. [26] studied the passivation and the resistance to pitting corrosion of duplex stainless steel in neutral and alkaline buffered solutions, with and without chloride ions. The presence of NaCl enhanced the metal's electrodissolution through the passive layer. Antony et al. [27] showed the aggressiveness of sulphate-reducing bacteria in a marine environment, which plays an important role in the corrosion of duplex. Jeffrey et al. [28] compared the corrosion behaviour of 2205 duplex stainless steel with AISI type 316L stainless steel in NaCl solution. Results show that 2205 has a longer passivation range and higher corrosion resistance than 316L. Siow et al. [29] studied the pitting corrosion of SAF2507, SAF2205 and SAF2304 duplex stainless steels by electrochemical tests and concluded that SAF2507 had the highest pitting corrosion resistance followed by SAF2205. Hussain and Robinson [30] studied the erosion–corrosion of 2205 duplex stainless steel in flowing seawater containing sand particles. Results showed that the highest erosion–corrosion rate occurred in the stagnation region, immediately beneath the jet, where sand particles impacted the surface. Wang et al. [31] showed that chloride ions had a strong effect on the nano-mechanical parameters of the corroded surface layer of 00Cr22Ni5Mo3N duplex stainless under cavitation in chloride solutions. Prawoto et al. [32] studied the effect of pH and chloride concentration on corrosion behaviour of duplex stainless steel UNSS32205 and concluded that decrease in pH and increase in temperature increases the corrosion rate of the steel at different solutions with different temperatures and periods of immersion with the pitting corrosion preferentially attacking the austenite phase of the steel. The corrosion of DIN 1.4035 martensitic stainless steel DIN 1.4035 in ethanol-containing gasoline mixtures with chloride and acetic acid concentrations was studied by Jörg and Sannakaisa [33] at room temperature. Pitting corrosion was detected at extremely low chloride-concentrations which propagated with increase in chloride concentration. Kimura et al. [34] studied the corrosion resistance of martensitic stainless steel OCTG was studied at a high CO_2 and simulated acidizing condition. No localized corrosion was observed during the exposure hours. The pitting corrosion resistance of 16Cr-2 Ni steels after austenitizing at various temperatures followed by double tempering was studied by Rajasekhar and Reddy [35]. The results show that double austenitization followed by double tempering resulted high pitting corrosion resistance as compared to single austenitization temperatures. The electrochemical corrosion behaviour of martensitic-austenitic stainless steel was investigated in 0.5, 1, 3 and 5 wt.% HCl solutions. Results show that the increase of acid concentration shifts the corrosion potential to more negative values and increasing the corrosion current and pitting corrosion was observed [36]. This research aims to study and compare the electrochemical corrosion behaviour of S32101 duplex stainless steel and 410 martensitic stainless steel specific concentrations of HCl acid for application in crude distillation overhead systems in petrochemical refinery.

2. Materials and methods

2.1. *Material*

S32101 duplex (DSS) and 410 martensitic (MSS) stainless steels purchased from the Steel Works, Owode, Nigeria and analysed at the Materials Characterization Laboratory, Department of

Please cite this article in press as: Loto RT. Study of the corrosion behaviour of S32101 duplex and 410 martensitic stainless steel for application in oil refinery distillation systems. J Mater Res Technol. 2016. http://dx.doi.org/10.1016/j.jmrt.2016.11.001

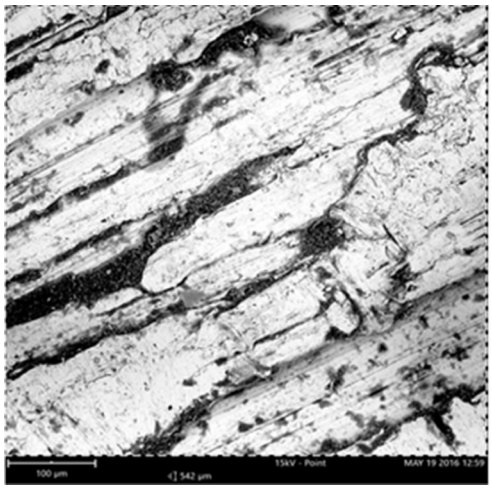

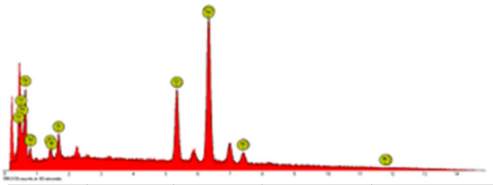

Element number	Element symbol	Element name	Confidence	Concentration (%)
26	Fe	Iron	100.0	61.2
24	Cr	Chromium	100.0	22.8
14	Si	Silicon	100.0	1.6
28	Ni	Nickel	100.0	8.8
35	Br	Bromine	100.0	1.2
42	MO	Molybdenum	100.0	2.5
61	Pm	Promethium	100.0	1.9

Fig. 1 – Micrograph of scanning electron microscopy and energy dispersive spectroscopy for S32101 duplex stainless steel.

Mechanical Engineering, Covenant gave an average nominal composition of nominal per cent (%) composition shown in the scanning electron microscopy micrographs in Figs. 1 and 2. The steels have a cylindrical dimension of 17 and 7 mm diameter respectively.

2.2. *Acid test solution*

Specific concentrations (1–6 M) of dilute HCl acid solution were prepared by dilution of an analytical grade of the (37%) with distilled water and used as the corrosive test environment to simulate the condition in the crude distillation overhead systems of oil refineries.

2.3. *Preparation of mild steel samples*

The stainless steels were machined into 6 test samples each for both steels. The average length of the duplex steel is 7 mm while the martensitic steel is 10 mm. The two exposed surface ends of the steel samples were metallographically prepared with silicon carbide abrasive papers of 80, 120, 220, 800 and 1000 grits before being polished with 6 μm diamond liquid, rinsed with distilled water and acetone, dried and later stored in a desiccator for weight-loss analysis and potentiodynamic polarization resistance technique in accordance with ASTM G1-03(2011) [37].

2.4. *Weight-loss analysis*

Weighed steel samples were individually immersed fully into 200 mL of the dilute HCl acid media for 432 h at ambient temperature of 25 °C [38]. Each sample was removed from the solution at 24 h interval, rinsed with distilled water and acetone, dried and re-weighed according to ASTM G31-12a [39]. Graphical illustrations of corrosion rate, γ (mm/y) versus exposure time T were plotted from the data obtained during the exposure hours. The corrosion rate (γ), mm/y calculation is defined as [40].

$$\gamma = \left[\frac{87.6w}{DAT}\right] \quad (1)$$

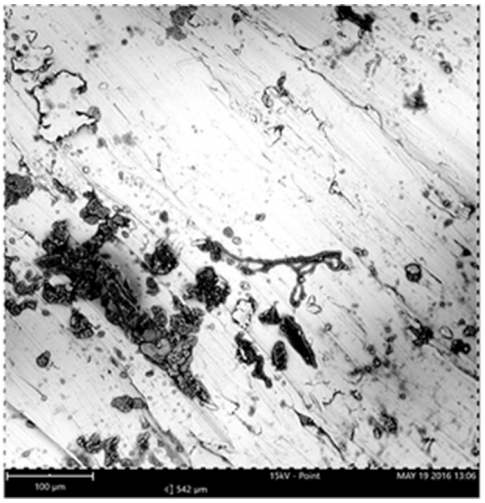

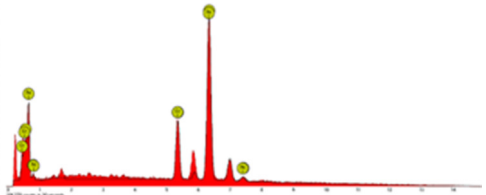

Element number	Element symbol	Element name	Confidence	Concentration (%)
26	Fe	Iron	100.0	79.5
24	Cr	Chromium	100.0	17.3
28	Ni	Nickel	100.0	1.5
14	Si	Silicon	100.0	1.7

Fig. 2 – Micrograph of scanning electron microscopy and energy dispersive spectroscopy for 410 martensitic stainless steel.

Please cite this article in press as: Loto RT. Study of the corrosion behaviour of S32101 duplex and 410 martensitic stainless steel for application in oil refinery distillation systems. J Mater Res Technol. 2016. http://dx.doi.org/10.1016/j.jmrt.2016.11.001

Table 1 – Data for DSS samples in dilute HCl from weight loss analysis.

Sample	Solution concentration (M)	Weight loss (g)	Corrosion rate (mm/y)
A	1 M	0.003	0.00001
B	2 M	0.076	0.00028
C	3 M	3.982	0.01492
D	4 M	6.267	0.02347
E	5 M	8.699	0.03258
F	6 M	12.245	0.04586

Table 2 – Data for MSS samples in dilute HCl from weight loss analysis.

Sample	Solution concentration (M)	Weight loss (g)	Corrosion rate (mm/y)
A	1 M	0.001	0.062
B	2 M	0.050	2.787
C	3 M	0.050	2.788
D	4 M	0.048	2.655
E	5 M	0.048	2.672
F	6 M	0.051	2.827

where w is the weight loss in mg, D is the density in g/cm^3, A is the total area in cm^2 and 87.6 is a constant.

2.5. *Potentiodynamic polarization technique*

Potentiodynamic polarization test was performed with the two different cylindrical stainless steel electrodes mounted in acrylic resin with an unconcealed surface area of 154 mm^2. The steel electrode was prepared according to ASTM G59-97(2014) [41]. The studies were performed at 25 °C ambient temperature with Digi-Ivy 2300 potentiostat and electrode cell containing 200 mL of the acid media. Platinum was used as the counter electrode and silver chloride electrode (Ag/AgCl) was employed as the reference electrode. Potentiodynamic measurement was performed from −1.5 V to +1.5 V at a scan rate of 0.0016 V/s according to ASTM G102-89(2015) [42]. The corrosion current density (j_{corr}) and corrosion potential (E_{corr}) were calculated from the Tafel plots of potential versus log current. The corrosion rate (γ) and the percentage inhibition efficiency (η_2) were from Eq. (2).

$$\gamma = \frac{0.00327 \times J_{corr} \times E_q}{D} \quad (2)$$

where j_{corr} is the current density in μA/cm^2, D is the density in g/cm^3; E_q is the specimen equivalent weight in grams. 0.00327 is a constant for corrosion rate calculation in mm/y [43,44].

2.6. *Scanning electron microscopy and energy dispersive spectroscopy*

The electron micrographs of surface topography of the uninhibited and inhibited stainless steel surfaces were obtained and studied after weight-loss analysis with the aid of Phenom-World scanning electron microscope.

3. Results and discussion

3.1. *Weight-loss measurements*

Data obtained from weight loss measurement for weight loss (w) and corrosion rate (γ) for DSS and MSS in HCl acids are shown in Tables 1 and 2. Fig. 3a and b shows the plot of corrosion rate against immersion time in the acid media for the two steels. Both steel samples corroded in varying degree in the acid media. The steel being ferrous alloys spontaneously reacts with HCl acid resulting in hydrogen evolution and

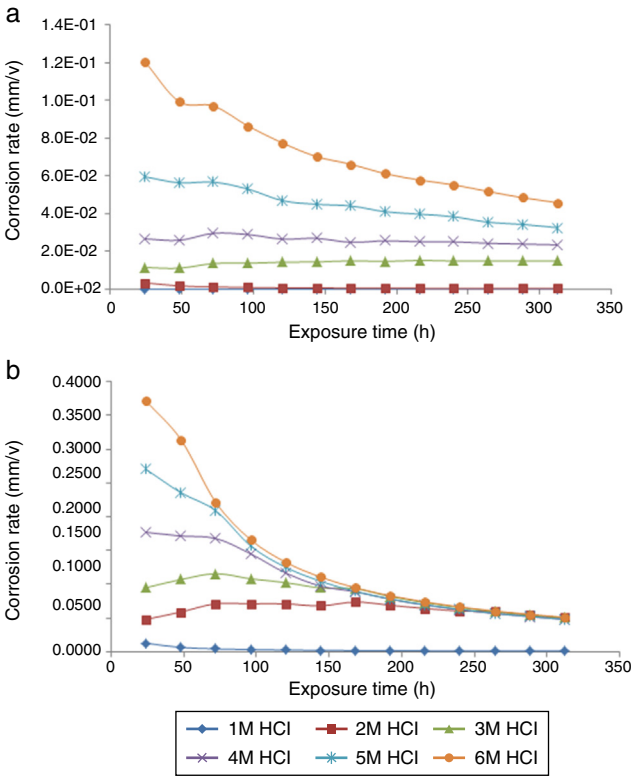

Fig. 3 – Plot of (a) corrosion rate versus exposure time for DSS samples in HCl acid, (b) plot of (a) corrosion rate versus exposure time for MSS samples in HCl acid.

oxidation reactions causing the release of Fe^{2+} ions into the solution as described by the following equation of reaction;

$$Fe + 2H^+ = Fe^{2+} + H_2 \quad (3)$$

The electrochemical reaction consist of two separate processes

(a) Metal (anodic) dissolution process
This is the oxidation of the metal which involves the generation of metallic ions which passes into the solution and the release of electrons according to Eq. (4).

$$Fe = Fe^{2+} + 2e^- \quad (4)$$

(b) Hydrogen evolution reaction

Please cite this article in press as: Loto RT. Study of the corrosion behaviour of S32101 duplex and 410 martensitic stainless steel for application in oil refinery distillation systems. J Mater Res Technol. 2016. http://dx.doi.org/10.1016/j.jmrt.2016.11.001

This is the cathodic process involving the reduction of protons.

$$2H^+ + 2e^- = H_2 \quad (5)$$

(c) Oxygen reduction reaction.
The acid solution being diluted in H_2O, oxygen is present in dissolved amount which is reduced during the corrosion process according to Eq. (6).

$$O_2 + 4H^+ + 4e^- = H_2O \quad (6)$$

The reaction occurs at different locations on the steel surfaces especially sites or regions of flaws, non-metallic inclusions, defects, etc. Observation of Table 1 shows a gradual increase in corrosion rate for DSS samples with increase in HCl acid concentration; however the corrosion rate values are generally insignificant from the perspective of alloy degradation as DSS proves to be strongly resistant to corrosion especially the electrochemical action of chloride ions responsible for general and localized corrosion reactions. The corrosion behaviour of the DSS samples in 1–6 M HCl acid concentration are clearly distinct in Fig. 3a, the DSS sample in 6 M and 5 M HCl acid had the highest corrosion rate consecutively throughout the exposure hours; however, the corrosion rate decreased significantly with time due to the strong resilient passive film which reforms on the steel surface and slowed down the corrosion reactions. The corrosion rate from 1 M to 4 M remained generally constant throughout with DSS samples in 1–2 M HCl acid exhibiting the lowest corrosion rates. Their corrosion rates are generally insignificant and the steel samples were relatively corrosion resistant and electrochemically stable throughout.

Observation of the graphical plot in Fig. 3b shows the corrosion behaviour of MSS in HCl which is slightly similar to DSS. The corrosion rates of MSS samples in 4–6 M HCl acid concentration decreased significantly during the exposure hours while the corrosion rates of samples in 1–3 M HCl acid concentration remained generally the same throughout in the acid solution; however the MSS sample in 1 M HCl acid had the lowest corrosion rate. The corrosion rate values of MSS samples are significantly higher than the values for DSS samples on comparison of the values from Tables 1 and 2 despite their similar electrochemical behaviour in HCl.

Increasing in chloride content due to increase in concentration of the acid solution did not result in significant decrease in the strength of the passive film as the metal electro-dissolution did not dominate the corrosion reaction mechanism though this was observed for MSS samples, but DSS samples proved the opposite due to their very low corrosion rate which at some concentration was very insignificant. Previous research concludes that chloride ions penetrate through the passive films of stainless steel with appreciable chromium content, and upon reaching the metal/film interface, results in film breakdown [44–48], but DSS samples demonstrates strong resistance to general corrosion and hence electrochemical deterioration due to chloride ions. The corrosion resistance of DSS samples is due to the presence of chromium oxides within the protective film as a result of its higher chromium content when compared to MSS. It is believed that the chromium content caused the formation of insoluble Cr_2O_3, which hindered the deterioration of the alloy [49].

3.2. *Potentiodynamic polarization test*

The potentiodynamic polarization behaviour of DSS and MSS samples in HCl acid concentrations is presented in Figs. 4 and 5. Tables 3 and 4 show the results obtained from the anodic and cathodic polarization scans. Observation of Table 3 shows the remarkable difference in corrosion rate values between DSS samples for 1–2 M and 3–6 M HCl concentrations for which there was a significant increase in corrosion rate with respect to increase in HCl acid concentrations. The stainless steel being heterogeneous in nature from observation of EDS micrographs (Figs. 1 and 2) has specific sites on its surface which are oxidized in the acid solution possibly causing the formation of porous oxides and pits due to the depassivation effect in iron dissolution within the alloy substrate or breakdown of passivity on the stainless steel. The increased presence of corrosive ions within the acid solution accelerated the corrosion rate after 2 M HCl concentration causing the formation of pores and channels within the oxide layer which lead to further corrosion. Metallic corrosion is complex and non-homogeneous due to the presence of numerous anodic and cathodic reaction cells. The presence of chloride ions

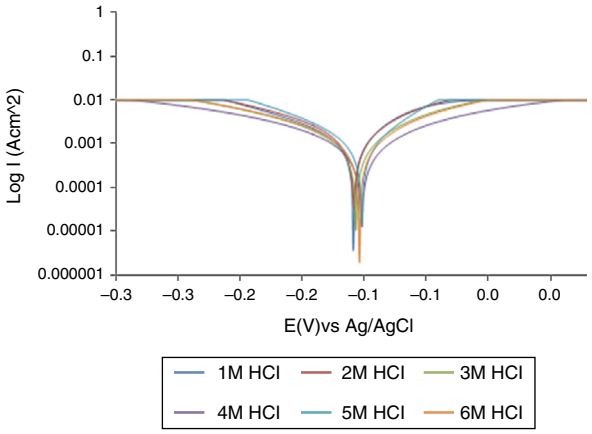

Fig. 4 – Polarization plot for DSS in 1–6 M HCl.

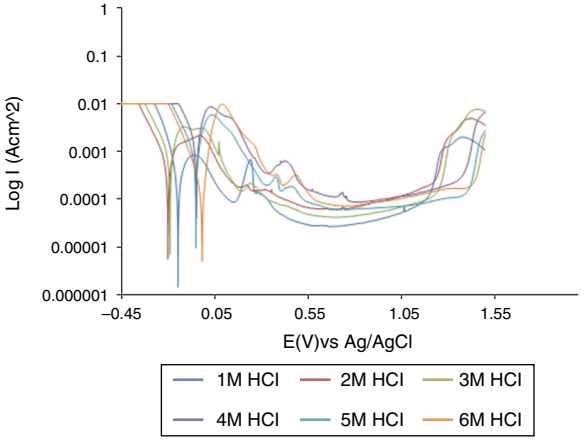

Fig. 5 – Polarization plot for MSS in 1–6 M HCl.

Please cite this article in press as: Loto RT. Study of the corrosion behaviour of S32101 duplex and 410 martensitic stainless steel for application in oil refinery distillation systems. J Mater Res Technol. 2016. http://dx.doi.org/10.1016/j.jmrt.2016.11.001

Table 3 – Potentiodynamic polarization results for DSS in 1–6 M HCl.

HCl concentration (M)	Corrosion rate (mm/y)	Corrosion current (A)	Corrosion current density (A/cm^2)	Corrosion potential (V)	Polarization resistance, R_p (Ω)	Cathodic Tafel slope, B_c (V/dec)	Anodic Tafel slope, B_a (V/dec)
1	0.046	1.10E−05	4.31E−06	−0.139	12.26	−8.345	3.988
2	0.052	1.23E−05	4.85E−06	−0.138	11.51	−7.258	4.127
3	0.112	2.64E−05	1.04E−05	−0.137	16.69	−7.130	7.442
4	0.160	3.78E−05	1.49E−05	−0.132	23.69	−6.725	6.867
5	0.225	5.31E−05	2.09E−05	−0.132	13.49	−9.268	0.020
6	0.234	5.52E−05	2.17E−05	−0.134	16.89	−7.176	7.563

Table 4 – Potentiodynamic polarization results for MSS in 1–6 M HCl.

HCl concentration (M)	Corrosion rate (mm/y)	Corrosion current (A)	Corrosion current density (A/cm^2)	Corrosion potential (V)	Polarization resistance, R_p (Ω)	Cathodic Tafel slope, B_c (V/dec)	Anodic Tafel slope, B_a (V/dec)
1	1.46	6.65E−05	1.33E−04	−0.148	55.08	−11.370	1.271
2	17.54	8.00E−04	1.60E−03	−0.202	32.11	−8.027	1.581
3	18.19	8.30E−04	1.66E−03	−0.191	18.98	−7.931	−0.350
4	17.78	8.11E−04	1.62E−03	−0.050	9.34	−7.819	0.691
5	16.24	7.41E−04	1.48E−03	−0.052	17.83	−8.218	2.636
6	19.84	9.05E−04	1.81E−03	−0.019	83.62	−10.480	11.470

significantly influence the corrosion behaviour of the steel due to their ability to penetrate easily into the protective oxide film, thereby breaking its passivity under induced potential which creates a high electric field across this film during potentiostatic scanning, however the corrosion rates of DSS samples are relatively low [50].

The samples displayed similar electrochemical behaviour over the potential domain from observation of the polarization plot in Fig. 4 and the anodic/cathodic Tafel constants in Table 3. The anodic and cathodic reaction mechanisms remained generally the same at all HCl concentrations. Increase in corrosion current density observed on the plot is as a result of active metal dissolution reaction of the passive film and minimal pit initiation. DSS did not display any passivation behaviour related to pitting corrosion resistance in the polarization plot though this has minor effect on its general corrosion behaviour. The alloy remained active over the potential range and shows little passivity from observation of its corrosion potentials which remained generally the same [51]. The cathodic and Tafel constants in Table 3 did not show any usual activity, but there seems to be a consistent interaction between the anodic and cathodic potentials of the corrosion mechanism at all HCl concentrations. The corrosion majorly responsible seems to general corrosion over the entire alloy surface. The presence of ferrite in DSS is responsible for the refined grain of both the austenite and the ferrite phases in DSS, and is suggested to be less resistant to pitting corrosion [52,6]. There are circumstances in which different phase transformations such as those responsible for the sigma phase do occur, which make the steel susceptible to localized corrosion. The relatively low corrosion rate of DSS when compared to MSS (Table 4) shows that most of its alloying elements are less noble than the iron metal substrate, thus they tend to dissolve sacrificially during polarization. The products of the electrochemical process are responsible for the protective film resistant to corrosion as it limits the diffusion of corrosive ions from the electrolyte to the metal surface [2,53].

The corrosion behaviour of MSS observed on the polarization plot in Fig. 5 significantly contrasts the behaviour of DSS samples in addition to its significantly higher corrosion rates. Active competition between the anodic and cathodic reaction mechanisms is clearly visible from observation of the anodic/cathodic Tafel constants in Table 4 at all HCl concentrations. At 1–2 M HCl acid concentration cathodic polarization (involving oxygen reduction and hydrogen evolution reactions) dominated the redox corrosion processes from observation of the corrosion potentials after which anodic polarization (alloy dissolution) dominated till 6 M HCl acid concentration. Though the MSS samples showed active corrosion above 1 M HCl acid concentration, the steel samples displayed strong resistance to localized corrosion reactions i.e. pitting due to the passive behaviour shown in the polarization plot. Its metallurgical structure and chromium content enhanced the steel passivation through the formation of Fe-Cr oxychloride salt films at the interface of the alloy under which passive films are formed. The change at the metal/solution interface from active deterioration to the passive state generally started about at 0.220 V till about 1.330 V for all MSS samples (Fig. 5) after which the alloy transits to the transpassive region in the polarization plot within the potential range of 1.180–1.340 V before completely failing at 1.500 V which corresponds to a current density range of 0.000873–0.00678 A/cm^2.

Increase in HCl concentration did not cause any significant decrease in the potential range for passivity for MSS as the metal electro-dissolution process was hindered. This is confirmed from the corrosion rate and corrosion potential values which showed active passive electrochemical behaviour, thus MSS displayed strong resistance to localized and general corrosion as it delayed the formation of pits and specimen failure. Breakdown of its passive film can be seen to be partially

Please cite this article in press as: Loto RT. Study of the corrosion behaviour of S32101 duplex and 410 martensitic stainless steel for application in oil refinery distillation systems. J Mater Res Technol. 2016. http://dx.doi.org/10.1016/j.jmrt.2016.11.001

dependent on the circumstances associated with pitting corrosion. The passive region in all cases extends up to a certain critical potential, at which the small passive current density increases rapidly indicating initiation of pitting corrosion. Once a pit nucleates, pit growth and propagation proceeds in active dissolution mode just before the transpassive region of the polarization plot. At the critical potential the passive film perforates/breaks due to chloride penetration/adsorption causing alloy dissolution [54–58]. Despite its remarkable resistance to localized corrosion, the passivation behaviour of MSS only tends to delay the onset of active metal dissolution; the steel eventually fails at higher corrosion rates.

3.3. *Scanning electron microscopy and energy dispersive spectroscopy*

The micrographs of scanning electron microscopy and energy dispersive spectroscopy for DSS and MSS samples after the corrosion tests are shown in Figs. 6–9. Observation of Fig. 6 shows the marginal change in surface topography and morphology of the DSS sample in comparison to the control sample (Fig. 1). The percentage nominal composition of the main alloying elements responsible for corrosion resistance has decreased slightly due to the degradation effect of the corrosive anions. This is responsible for the change in the morphology of the sample due to the of e metal ions into the acid solution. As a result there is a mild increase in the composition of the main iron substrate; however DSS maintains its passivity. The micrograph of Fig. 8 is a higher magnification of Fig. 6 where the corrosion pits are clearly visible. Energy dispersive spectroscopy of the pits shows a lower composition of the main alloying elements of DSS.

The MSS micrograph shown in Fig. 7 sharply contrasts the control sample in Fig. 2 and DSS micrograph in Fig. 6. Numerous corrosion pits and severe morphological deterioration are clearly visible as a result of the electrochemical action of corrosive ions present in the acid media. The anions react with the metal surface through the redox corrosion mechanism resulting in the loss of valence electrons and passage of Fe^{2+} cations into the acid solution. The main alloying elements have significantly declined in percentage composition leaving an increased percentage composition of iron. The

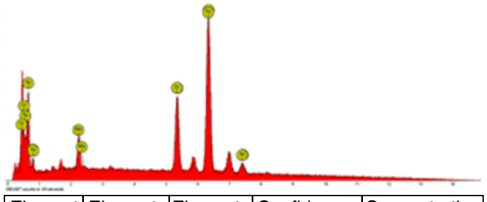

Element number	Element symbol	Element name	Confidence	Concentration (%)
26	Fe	Iron	100.0	67.8
24	Cr	Chromium	100.0	19.7
42	MO	Molybdenum	100.0	1.6
28	Ni	Nickel	100.0	6.9

Fig. 6 – Micrograph of scanning electron microscopy and energy dispersive spectroscopy for DSS sample after corrosion test.

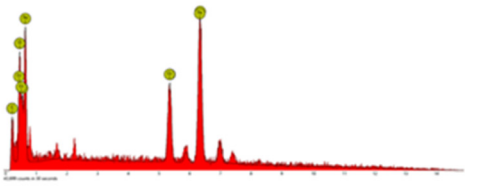

Element number	Element symbol	Element name	Confidence	Concentration (%)
26	Fe	Iron	100.0	79.4
24	Cr	Chromium	100.0	14.1
6	C	Carbon	100.0	6.5

Fig. 7 – Micrograph of scanning electron microscopy and energy dispersive spectroscopy for MSS samples after corrosion test.

Please cite this article in press as: Loto RT. Study of the corrosion behaviour of S32101 duplex and 410 martensitic stainless steel for application in oil refinery distillation systems. J Mater Res Technol. 2016. http://dx.doi.org/10.1016/j.jmrt.2016.11.001

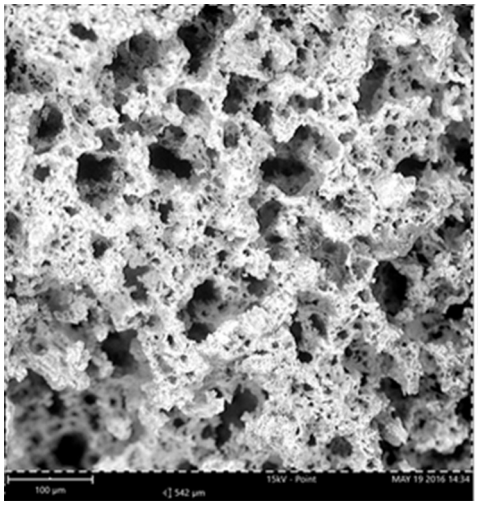

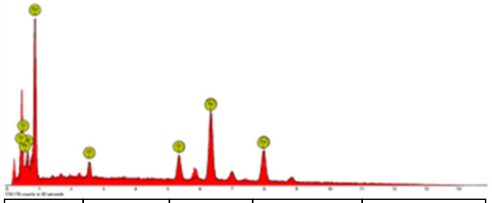

Element number	Element symbol	Element name	Confidence	Concentration (%)
26	Fe	Iron	100.0	81.4
29	Cu	Copper	100.0	3.4
24	Cr	Chromium	100.0	9.4
17	Cl	Chlorine	100.0	5.2
28	Ni	Nickel	100.0	0.6

Fig. 8 – Micrograph of scanning electron microscopy and energy dispersive spectroscopy for DSS pitted region.

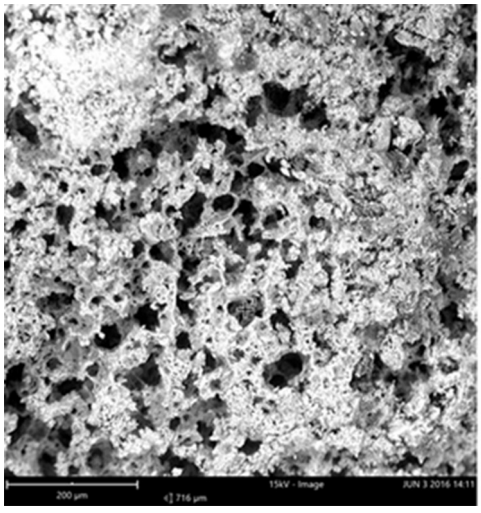

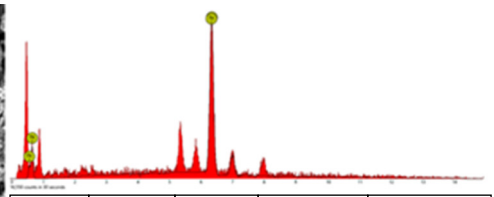

Element number	Element symbol	Element name	Confidence	Concentration (%)
26	Fe	Iron	100.0	89.0
29	Cu	Copper	100.0	1.3
24	Cr	Chromium	100.0	5.1
17	Cl	Chlorine	Manual	4.4
28	Ni	Nickel	Manual	0.2

Fig. 9 – Micrograph of scanning electron microscopy and energy dispersive spectroscopy for MSS pitted region.

micrographic image confirms the results from weight loss and potentiodynamic polarization test. The micrograph of Fig. 9 shows a higher magnification of Fig. 7, revealing the corrosion pits. Energy dispersive spectroscopy of the corrosion pits gave a lower percentage composition of the alloying elements than DSS sample indicating a more severe corrosion occurring in the corrosion pits in MSS.

In the acid test solution, anodic polarization of the sample alloys leads to selective dissolution of iron and the alloying elements causing general and pitting corrosion. The location of pits is determined by the microstructure of the alloy and the presence of flaws, inclusion and impurities. Previous research has shown have shown that the regions of pit nucleation on passive alloy surfaces is generally related to the presence of defects and nonmetallic impurities [59,60]. The chloride ions in the solution also result in an even higher number of defects in the passive film. Within the pits, an extremely corrosive mini-environment is established, which bears little similarity to the bulk corrosive environment. Electrochemical reaction within the pit electrolyte increases in positive electrical charge in contrast to the electrolyte surrounding the pit. The positively charged pit attracts chloride ions which increases the acidity of the electrolyte. The danger of this process is the localized presence of pits which are clearly visible on MSS micrographs.

4. Conclusion

S32101 duplex stainless steel displayed stronger resistance to pitting and general corrosion when compared to 410 martensitic stainless steel in HCl solution due to its higher percentage composition of chromium, nickel and other alloying elements. Its surface morphology was far less corroded with fewer number of corrosion pits than the 410 martensitic steel as a result of the durability of its passive film from its higher chromium content. The martensitic steel displayed passivity behaviour during potentiodynamic polarization with unstable corrosion

Please cite this article in press as: Loto RT. Study of the corrosion behaviour of S32101 duplex and 410 martensitic stainless steel for application in oil refinery distillation systems. J Mater Res Technol. 2016. http://dx.doi.org/10.1016/j.jmrt.2016.11.001

reaction mechanisms however its corrosion rates were significantly higher than values obtained for S32101 duplex steel which showed stable electrochemical behaviour making it suitable for application as crude distillation overhead systems.

Conflicts of interest

The authors declare no conflict of interest.

REFERENCES

[1] Hashimoto K, Asami K, Kawashima A, Habazaki H, Akiyama E. The role of corrosion-resistant alloying elements in passivity. Corros Sci 2007;49(1):42–52.
[2] Laycock NJ, Newman RC. Localized dissolution kinetics, salt films, and pitting potentials. Corros Sci 1997;39(10–11):1771–90.
[3] Leckie HP, Uhlig HH. Environmental factors affecting the critical potential for pitting in 18-8 stainless steel. J Electrochem Soc 1966;113(12):1262–7.
[4] Llewellyn DT, Hudd RC. Steels: metallurgy and applications. 3rd ed. Oxford, UK: Butterworth-Heinemann; 1998.
[5] Sedano J, Curiel L, Corchado E, Cal E, Villar JR. A soft computing method for detecting lifetime building thermal insulation failures. Int Comput Aided Eng 2010;17(2):103–15.
[6] Sedriks AJ. Corrosion of stainless steel. New York, NY: John Wiley and Sons; 1996.
[7] Turtle RN. Corrosion in oil and gas production. J Petrol Technol 1987;1987(39):756–62.
[8] Jones LW. Corrosion and water technology for petroleum producers; 1998. Tulsa, Oklahoma.
[9] Bagdasarian A, Feather J, Hull B, Stephenson R, Strong R. Crude unit corrosion and corrosion control, Corrosion/96. Houston, TX: NACE International; 1996.
[10] Braden V, Petersen P, Malpiedi M, Bowerbank L, Gorman J. Crude unit overhead corrosion control, Corrosion/98. Houston, TX: NACE International; 1998.
[11] Duggan G, Rechtien R. Application of ionic equilibria process simulation for atmospheric distillation overhead systems, Corrosion/98. Houston, TX: NACE International; 1998.
[12] Valenzuela D, Dewan A. Refinery crude column overhead corrosion control, amine neutralizer electrolyte thermodynamics, thermochemical properties and phase equilibria. Fluid Phase Equilib 1998;(158–160):829–34.
[13] Coble ND. Corrosion philosophy: treat the source, not the symptom, Corrosion. NACE International; 2002.
[14] Saab MS, Dias OC, Faqeer FM. Damage mechanisms and corrosion control in a crude unit overhead line, Corrosion/05. Houston, TX: NACE International; 2005.
[15] Eaton P, Kaur H, Gray M. Factors affecting salt hydrolysis in heavy crude, Eurocorr/09; 2009. Nice, France.
[16] Kapusta S, Ooms A, Buijis JW, Fan D, Fort W III. Systematic approach to controlling fouling and corrosion in crude unit overheads and hydrotreater reactor effluents, Corrosion/01. Houston, TX: NACE International; 2001.
[17] Gutzeit J. Effect of organic chloride contamination of crude oil on refinery corrosion, Corrosion/00. Houston, TX: NACE International; 2000.
[18] Gutzeit J. Controlling crude unit overhead corrosion – rules of thumb for better crude desalting, Corrosion/07. Houston, TX: NACE International; 2007.
[19] Shetty SD, Shetty P, Nayak HVS. The inhibition action of N-(furfuryl)-N′-phenyl thiourea on the corrosion of mild steel in acid media. J Serb Chem Soc 2006;7(10):1073.
[20] Crude distillation unit—distillation tower overhead system corrosion; 2009. NACE 34109-2009.
[21] Schutt HU, Horvath RJ. Crude column overhead corrosion problem caused by oxidized sulfur species, Corrosion/87. Houston, TX: NACE International; 1987.
[22] Schofield MJ. Plant engineer's reference book. Elsevier; 2003.
[23] Charles J. Composition and properties of duplex stainless steels. Weld World 1995;36:89–97.
[24] Àabanowski J. Duplex stainless steels – new material for chemical industry. Appar Chem Eng 1997;36(2):3–10.
[25] Brickner KG. Stainless steel for room and cryogenic temperatures. Met Eng Q 1968:25.
[26] Souto RM, Mirza RIC, Gonzales S. Resistance to localized corrosion of passive films on a duplex stainless steel. Corrosion 2001;57:195–9.
[27] Antony PJ, Chongdar S, Kumar P, Raman R. Corrosion of 2205 duplex stainless steel in chloride medium containing sulfate-reducing bacteria. Electrochim Acta 2007;52:3985–94.
[28] Jeffrey AP, Guzman A, Zuccari A, David WT, Rhodes BF, Oshida Y, et al. Corrosion behavior of 2205 duplex stainless steel. Am J Orthod Dentofac Orthop 1997;112(1):69–79.
[29] Siow KS, Song TY, Qiu JH. Pitting corrosion of duplex stainless steels. Anti-Corros Methods Mater 2001;48(1):31–7.
[30] Hussain EAM, Robinson MJ. Erosion–corrosion of 2205 duplex stainless steel in flowing seawater containing sand particles. Corros Sci 2007;49(4):1737–54.
[31] Wan T, Xiao N, Shen H, Yong X. The effect of chloride ions on the corroded surface layer of $Cr_{22}Ni_5Mo_3N$ duplex stainless steel under cavitation. Ultrason Sonochem 2016;33:1–9.
[32] Prawoto Y, Ibrahim K, Wan Nik WB. Effect of ph and chloride concentration on the corrosion of duplex stainless steel. Arab J Sci Eng 2009;34(2C):115–27.
[33] Jörg A, Sannakaisa V. Corrosion of martensitic stainless steel in ethanol-containing gasoline: influence of contamination by chloride, H_2O and acetic acid. Corros Sci 2015;98:318–26.
[34] Kimura M, Sakata K, Shimamoto K. Corrosion resistance of martensitic stainless steel OCTG in severe corrosion environments, Corrosion/07, 11–15 March. Nashville, TN, USA: NACE International; 2007.
[35] Rajasekhar A, Reddy GM. The effect of single and double austenitization temperatures on the microstructure, mechanical properties and pitting corrosion of AISI electron beam welds. J Mater Des Appl 2010;224:9–18.
[36] Sadawy MM, Shirinov TU, Heseinov RG. Corrosion and electrochemical behavior of martensitic–austenitic stainless steel in hydrochloric acid solutions. Int J Pure Appl Chem 2011;6(3):319–22.
[37] ASTM G1-03. Standard Practice for Preparing, Cleaning, and Evaluating Corrosion Test Specimens; 2011. Available at http://www.astm.org/Standards/G1.
[38] Mathur PB, Vasudevam T. Reaction rate studies for the corrosion of metals in acids. I: iron in mineral acids. Corrosion 1982;38(3):171–8.
[39] ASTMG31-12a. Standard Guide for Laboratory Immersion Corrosion Testing of Metals; 2012. Available at http://www.astm.org/Standards/G31.
[40] Loto RT, Ozcan E. Corrosion resistance studies of austenitic stainless steel grades in molten zinc-aluminum alloy galvanizing. J Fail Anal Prev 2016;16(3):427–37.
[41] ASTM G59-97. Standard Test Method for Conducting Potentiodynamic Polarization Resistance Measurements; 2014. Available at http://www.astm.org/Standards/G31/.
[42] ASTM G102-89. Standard Practice for Calculation of Corrosion Rates and Related Information from Electrochemical Measurements; 2015. Available at http://www.astm.org/Standards/G31.
[43] Sethi T, Chaturvedi A, Mathur RK. Corrosion inhibitory effects of some Schiff's bases on mild steel in acid media. J Chil Chem Soc 2007;3(52):1206–13.

Please cite this article in press as: Loto RT. Study of the corrosion behaviour of S32101 duplex and 410 martensitic stainless steel for application in oil refinery distillation systems. J Mater Res Technol. 2016. http://dx.doi.org/10.1016/j.jmrt.2016.11.001

[44] Ahmad K. Principles of corrosion engineering and corrosion control. Oxford, UK: Butterworth-Heinemann; 2006.
[45] Dong J, Zhou J. An investigation of pitting initiation mechanism of $Cr_{12}Ni_2W_1Mo_1V$ steel after induction hardening. J Mater Sci 2000;35:2653–7.
[46] Strehblow HH, Marcus P, Oudar J. Corrosion mechanisms in theory and practice. New York: Marcel Dekker; 1995.
[47] Hoar TP, Mears DC, Rothwell GP. The relationships between anodic passivity, brightening and pitting. Corros Sci 1965;5:279–89.
[48] Bentour A, Diamond S, Berke NS. Steel corrosion in concrete. London, UK: Chapman & Hall; 1997.
[49] Brooks AR, Clayton CR, Doss K, Lu YC. On the role of Cr in the passivity of stainless steel. J Electrochem Soc 1986;133:2459–64.
[50] Kocijan A, Donik C, Jenko M. Electrochemical and XPS studies of the passive film formed on stainless steels in borate buffer and chloride solutions. Corros Sci 2007;49:2083–98.
[51] Jones DA. Principles and prevention of corrosion. 2nd ed. Prentice Hall; 1996.
[52] Truman JE. Metall Mater Technol. 1980;2:75.
[53] Galvele JR. Transport processes in passivity breakdown—II. Full hydrolysis of the metal ions. Corros Sci 1981;21:551.
[54] Bohni H, Stockert L. The importance of metastable pitting high alloy steels. Mater Corros 1989;11:63–71.
[55] Yang Q, Luo JL. Effects of hydrogen and tensile stress on the breakdown of passive films on type 304 stainless steel. Electrochim Acta 2001;46:851–9.
[56] Abd El Meguid EA, Mahmoud NA, Abd El Rehim SS. Materials and corrosion. Mater Chem Phys 2000;63:67–74.
[57] Baboian R, Treseder RS. NACE Corrosion Engineer's Reference Book. NACE International; 2002.
[58] Hashimoto K, Asami K, Naka M, Masumoto T. The role of alloying elements in improving the corrosion resistance of amorphous iron base alloys. Corros Sci 1979;19(7):857–67.
[59] Garz I, Worch H, Schatt W. Studies on the anodic dissolution and the pitting corrosion of single-crystal nickel electrodes. Corros Sci 1969;9:71–2.
[60] Streicher MA. Pitting corrosion of 18Cr-8Ni stainless steel. J Electrochem Soc 1956;103:375.

Please cite this article in press as: Loto RT. Study of the corrosion behaviour of S32101 duplex and 410 martensitic stainless steel for application in oil refinery distillation systems. J Mater Res Technol. 2016. http://dx.doi.org/10.1016/j.jmrt.2016.11.001